International Immunology, Vol. 36, No. 7, pp. 339–352
https://doi.org/10.1093/intimm/dxae012
Advance Access publication 2 March 2024

Acute malaria suppresses the B lymphocytic niche in the bone marrow through the alteration of CXCL12-abundant reticular cells

Michelle Sue Jann Lee[1,2], Julia Matsuo-Dapaah[1], Camila Del Rosario Zorrilla[1], Yoshiki Omatsu[3,4], Takashi Nagasawa[3,4], Shun Uemura[5], Atsushi Iwama[5,6,7], Ken J. Ishii[2,7,8,9] and **Cevayir Coban[1,2,7,9]**

[1]Division of Malaria Immunology, Department of Microbiology and Immunology, The Institute of Medical Science (IMSUT), The University of Tokyo, 4-6-1 Shirokanedai, Minato-ku, Tokyo 108-8639, Japan
[2]International Vaccine Design Center, The Institute of Medical Science (IMSUT), The University of Tokyo, Tokyo 108-8639, Japan
[3]Laboratory of Stem Cell Biology and Developmental Immunology, Graduate School of Frontier Biosciences and Graduate School of Medicine, Osaka University, Osaka 565-0871, Japan
[4]Laboratory of Stem Cell Biology and Developmental Immunology, WPI Immunology Frontier Research Center (IFReC), Osaka University, Osaka 565-0871, Japan
[5]Division of Stem Cell and Molecular Medicine, Center for Stem Cell Biology and Regenerative Medicine, The Institute of Medical Science (IMSUT), The University of Tokyo, Tokyo 108-8639, Japan
[6]Laboratory of Cellular and Molecular Chemistry, Graduate School of Pharmaceutical Sciences, The University of Tokyo, Tokyo 113-0033, Japan
[7]The University of Tokyo Pandemic Preparedness, Infection and Advanced Research Center (UTOPIA), The University of Tokyo, Tokyo 108-8639, Japan
[8]Division of Vaccine Science, Department of Microbiology and Immunology, The Institute of Medical Science (IMSUT), The University of Tokyo, Tokyo 108-8639, Japan
[9]WPI Immunology Frontier Research Center (IFReC), Osaka University, Osaka 565-0871, Japan

Correspondence to: M. S. J. Lee; E-mail: msj-lee@ims.u-tokyo.ac.jp and C. Coban; E-mail: ccoban@ims.u-tokyo.ac.jp

Received 28 December 2023, *editorial decision* 27 February 2024, *accepted* 28 February 2024

Abstract

Bone marrow is a dynamic organ composed of stem cells that constantly receive signals from stromal cells and other hematopoietic cells in the niches of the bone marrow to maintain hematopoiesis and generate immune cells. Perturbation of the bone marrow microenvironment by infection and inflammation affects hematopoiesis and may affect immune cell development. Little is known about the effect of malaria on the bone marrow stromal cells that govern the hematopoietic stem cell (HSC) niche. In this study, we demonstrate that the mesenchymal stromal CXCL12-abundant reticular (CAR) cell population is reduced during acute malaria infection. The reduction of CXCL12 and interleukin-7 signals in the bone marrow impairs the lymphopoietic niche, leading to the depletion of common lymphoid progenitors, B cell progenitors, and mature B cells, including plasma cells in the bone marrow. We found that interferon-γ (IFNγ) is responsible for the upregulation of Sca1 on CAR cells, yet the decline in CAR cell and B cell populations in the bone marrow is IFNγ-independent. In contrast to the decline in B cell populations, HSCs and multipotent progenitors increased with the expansion of myelopoiesis and erythropoiesis, indicating a bias in the differentiation of multipotent progenitors during malaria infection. These findings suggest that malaria may affect host immunity by modulating the bone marrow niche.

Graphical Abstract

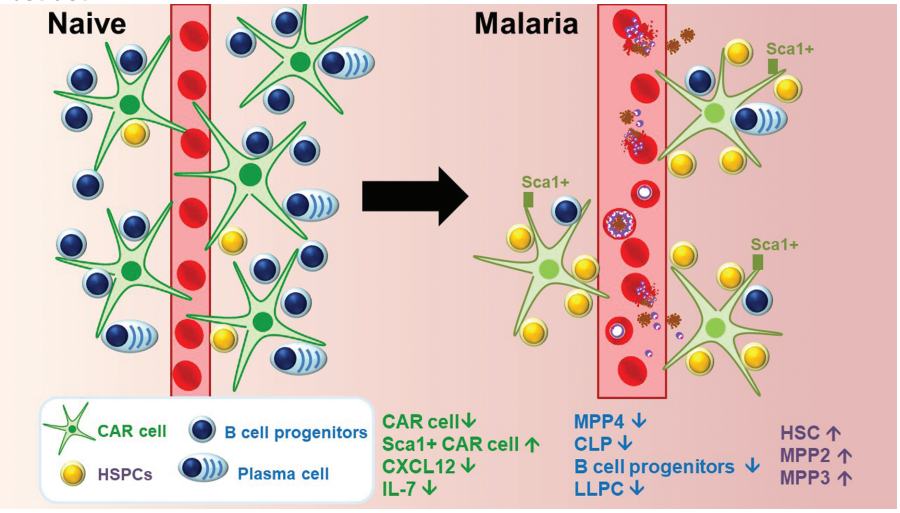

Keywords: bone marrow niche, hematopoiesis, IFNγ, lymphocyte, *Plasmodium*

Introduction

The global malaria control programs and surveillance efforts such as vector control, antimalarial drugs, and the recent rollout of malaria RTS,S vaccine with only modest efficacy contributed to the reduction of mortality caused by malaria to less than a million cases annually (1). However, the disease burden still remains high with more than 200 million cases of new infections per annum. Among the challenges to malaria eradication are the strategies of the malaria parasite, *Plasmodium* spp., to evade the host immune system, which prevents the host from acquiring sterile immunity and allows the parasite to continue subsequent transmissions (2). Field studies provide evidence that malaria modulates host immunity to other infections and responses to vaccination, and all-cause morbidity declines after malaria infections decrease (3, 4). Although antimalarial treatments can cure most cases of malaria, the disease can also lead to chronic tissue pathologies that increase susceptibility to other infections, osteoporosis, chronic anemia, neurological deficit, and gastrointestinal disorders (5, 6).

Bone marrow provides a niche for *Plasmodium* parasites to differentiate into sexual stage gametocytes for transmission (7), suggesting that the parasite manipulates the host bone marrow environment for its advantage. Many cell types within the bone marrow such as mesenchymal CXCL12-abundant reticular (CAR) cells, osteoblasts, endothelial cells, Schwann cells, regulatory T cells, and megakaryocytes play important roles in providing hematopoietic niches for the maintenance of hematopoietic stem cells (HSCs) and the development of immune cells (8). Stresses from infection, inflammation, and leukemia may alter or damage the hematopoietic niches (9). In the bone marrow, CXCL12 chemokine is highly expressed in perivascular CAR cells and low levels in endothelial cells and osteoblasts to recruit and maintain close proximity with hematopoietic stem/progenitor cells (HSPCs), common lymphoid progenitor (CLP), and B cell progenitors (8). CAR cells provide survival factors and various cytokines to these populations to maintain HSC quiescence and to regulate lineage development of multipotent progenitors (MPPs). Interleukin-7 (IL-7) is a key cytokine to drive lymphopoiesis and is mainly expressed by mesenchymal CAR cells in the bone marrow, although it is also expressed in low levels in other cells such as osteoblasts, sinusoidal endothelial cells, and periarteriolar pericytes (10). Both CXCL12 and IL-7 function synergistically for B cell development and plasma cell maintenance in the bone marrow (11, 12).

We previously found that acute non-lethal malaria infection depletes osteoblasts in the bone marrow (13). Another group recently showed that *Plasmodium berghei* ANKA that causes severe lethal malaria also depletes osteoblasts in the bone marrow and alters endothelial cell function, leading to increased HSC turnover and reduced HSC engraftment ability in the bone marrow (14). Although osteoblasts express very low levels of CXCL12, deletion of CXCL12 from osteoblasts in Col2.3-cre Cxcl12f/f mice resulted in a slight decrease in CLPs, despite having a normal frequency of B cell progenitors and other hematopoietic lineage compositions in the bone marrow (15). However, the deletion of CXCL12 from both osteoblasts and CAR cells in Prx1-cre Cxcl12f/f mice resulted in a severe reduction of CLP and B cell progenitors in the bone marrow (16). Moreover, osteoblast cell-specific deletion of IL-7 did not affect hematopoiesis and B lymphopoiesis, whereas IL-7 deletion from CAR cells led to depletion of CLPs in the bone marrow (10). This suggests that CAR cells are crucial in regulating B cell development and maintenance in the bone marrow. However, it remains unclear how malaria affects CAR cell populations in the bone marrow, and the role of CAR cells in regulating B lymphopoiesis and the retention of plasma cells in the bone marrow during malaria.

Methods

Mice

Six- to eight-week-old C57BL/6J wild-type mice were purchased from CLEA Japan. CXCL12-GFP mice were obtained from RIKEN #RBRC04200 (17). Interferon-γ

receptor (IFNγR)$^{-/-}$ mice were purchased from The Jackson Laboratory. IFNγR$^{-/-}$ CXCL12-GFP mice were generated by crossing IFNγR$^{-/-}$ mice with CXCL12-GFP mice. Age-matched mice were used as controls in every experiment. Animal experiments were conducted in accordance with institutional guidelines and approved by the review board for animal experiments of the Institute of Medical Science, The University of Tokyo.

Infection

Donor mice were made by infecting intraperitoneally *Plasmodium*-infected blood from frozen stock. Then, blood from a donor mouse was diluted with heparinized phosphate buffered saline (PBS) depending on the parasitemia. Mice were infected with either 2×10^5 infected red blood cells (iRBC) for *P. yoelii* non-lethal (*Py*NL) infection, 2×10^5 iRBC for *Plasmodium chabaudi* (*Pcc)* infection, or 1×10^6 iRBC for *P. berghei* ANKA (*Pb*A) infection (13). Parasitemia was monitored by Giemsa-stained blood smears.

Flow cytometry and cell sorting

Bone marrow cells were flushed from two femurs and two tibias with cold 2% fetal bovine serum (FBS) supplemented Dulbecco's Modified Eagle Medium (DMEM) containing 4.5 g/l glucose (Nacalai Tesque) on ice. For CAR cell staining, flushed bone marrow cells were digested with 5 mg/ml collagenase type I (Gibco) and 0.2 mg/ml DNase I (Sigma) with constant shaking at 37°C for 40 minutes. After digestion, bone marrow cells were gently resuspended. Single-cell suspensions were centrifuged at 2500 rpm at 4°C for 5 minutes. Cells were blocked with anti-mouse CD16/CD32 monoclonal antibody (eBioscience) for 10 minutes before subsequent staining with antibody cocktails for 30 minutes on ice. Dead cells were excluded using LIVE/DEAD Fixable Dead Cell Stain (Invitrogen). For CAR cell staining, cells were stained with PDGFRβ-biotin (R&D Systems), CD31 (PECAM-1)-PE-Cy7, CD45-PerCp/Cy5.5, CD19-AF700 (eBioscience), Sca1-BV785 (Biolegend) for 30 minutes on ice, followed by washing and subsequent staining with Streptavidin-BV421 (BD Bioscience) for another 30 minutes on ice.

For total bone marrow cell enumeration, bone marrow was flushed from femurs and tibias, and the leftover bone pieces were crushed with mortar and pestle, and subsequently filtered through a 70-μm cell strainer. For staining of hematopoietic cells, enzymatic digestion was omitted. Ammonium-Chloride-Potassium (ACK) lysis buffer (Lonza) was added to remove erythrocytes before antibody staining, except for the erythroid cell staining panel. In the HSPC panel, lineage cells were excluded using CD19-FITC, CD11b-FITC, CD3-FITC, Ter119-FITC, CD4-FITC, and B220-FITC (eBioscience). Antibodies for CD150-BV421, CD138-BV605, B220-BV510, CD24-PE, NK1.1-PE, CD44-PerCp/Cy5.5, CD49d-FITC, CD4-PE/Cy7, CD8-PE, TCRβ-Pacific blue, Ly6C-FITC, Ly6G-BV605, CD115-PE, CD19-APC, CD11b-PE/Cy7, Ter119-AF700, IgM-PerCp/Cy5.5 were from Biolegend. CD48-AF700, CD135 (Flt3)-PerCP-eFluor710, CD24-PE, CD43-FITC, IgD-eFluor 450, CD267 (TACI)-APC, IgA-PE, c-kit (CD117)-APC, CD127 (IL-7Rα)-PE were from eBioscience. IgG1-BV421 was from BD Bioscience, IgG2c-PE was from Southern Biotech. Cells were fixed with 2% paraformaldehyde (PFA) in PBS (Nacalai Tesque) for 15 minutes. At least 1 000 000 events gated on live cells were acquired using an LSRFortessa flow cytometer (BD Biosciences). Data were analyzed with FlowJo 10.9.0.

For cell sorting, bone marrow cells were collected from two femurs and two tibias per mouse. Live cells were sorted at 4°C on a BD FACSAria III Cell Sorter (BD Bioscience). Live cells were gated on CD45$^-$ Ter119$^-$ CD31$^-$ CXCL12$^+$ PDGFRβ$^+$ and then further sorted into either Sca1$^+$ or Sca1$^-$ populations.

Intracellular cytokine staining

Bone marrow cells were harvested and treated with ACK lysis buffer (Lonza). 2×10^6 cells were cultured in 0.2 ml DMEM containing 4.5 g/l glucose (Nacalai Tesque) supplemented with 10% FBS and 1% penicillin/streptomycin (Nacalai Tesque). Cells were cultured in the presence of BD GolgiPlug™ Protein Transport Inhibitor containing Brefeldin A (BD Biosciences) and with or without 20 ng/ml phorbol 12-myristate-13-acetate (PMA) and 1 μg/ml ionomycin for 3 hours. Cells were stained with anti-mouse CD16/CD32 (eBioscience) and subsequently with anti-mouse TCRβ-Pacific blue, CD4-FITC, NK1.1-PE, and CD8α-PE/Cy7 in diluted LIVE/DEAD Fixable Dead Cell Stain (Invitrogen). Cells were fixed with 2% PFA in PBS (Nacalai Tesque) for 20 minutes and permeabilized with Foxp3/Transcription Factor Permeabilization Buffer (eBioscience). Cells were intracellularly stained with anti-mouse IFNγ-APC (Biolegend). At least 200 000 events gated on live cells were acquired using an LSRFortesssa flow cytometer (BD Biosciences) and data were analyzed with FlowJo 10.9.0.

Enzyme-linked immunosorbent spot assay

Millipore MultiScreen$_{HTS}$ IP Filter Plates (Merck) were pretreated with 35% ethanol (Nacalai Tesque) and washed extensively with sterile water (Nacalai Tesque). Plates were coated with 2 μg/ml goat anti-mouse Ig, Human ads-UNLB (Southern Biotech) overnight at 4°C. Plates were blocked with DMEM complete medium containing 4.5 g/l glucose (Nacalai Tesque) supplemented with 10% FBS and 1% penicillin/streptomycin (Nacalai Tesque) for 3 hours at 37°C. Bone marrow cells were harvested and cultured in DMEM complete medium with a 1/2 serial dilution of cells starting from 1×10^6 cells per well at 37°C overnight. After subsequent washings with PBS followed by PBS with 0.01% Tween 20 (PBST), plates were incubated with goat anti-mouse IgA-HRP (Southern Biotech) or goat anti-mouse IgG-HRP (Southern Biotech) in PBS containing 1% FBS for 2 hours at room temperature. Plates were washed with PBST and then with PBS, before adding pre-filtered ready-to-use 3,3', 5,5"-tetramethylbenzidine (TMB) substrate for enzyme-linked immunosorbent spot (ELISpot) (MABTECH). Reactions were stopped by washing the plates extensively with MilliQ water. Images were captured using an ImmunoSpot Analyzer S6 Ultimate M2 (Cellular Technology Limited). The spot count was analyzed using ImmunoSpot 7.0.38.7 software.

Quantitative reverse transcription polymerase chain reaction

RNA was extracted from bone marrow cells from tibia or fluorescence-activated cell sorting (FACS)-sorted cells using TRIzol reagent (Invitrogen). Reverse transcription to cDNA was performed using ReverTra Ace qPCR RT Master Mix with gDNA remover (Toyobo). Quantitative PCR was performed using THUNDERBIRD Probe qPCR Mix (Toyobo) and Taqman primers for *Cxcl12*, *Il7*, *Kitl*, *Foxc1*, *Ebf3*, *Col3a1*, and *Ifng* (Applied Biosystems). Gene expressions were normalized to the expression levels of 18S rRNA.

Immunohistochemical analysis

Femurs were fixed in 4% PFA at 4°C overnight. Samples were washed with PBS before being transferred into 30% sucrose solution at 4°C overnight with constant shaking. Samples were cooled in dry ice-cooled hexane before being embedded in SCEM (Leica Microsystems) and were frozen using dry ice-cooled hexane. Frozen samples were sectioned at 20-μm thickness using Kawamoto's film method with Cryofilm type 3C from Section-lab. Bone sections were blocked with 3% donkey serum for 30 minutes at room temperature and stained with anti-endomucin (V.7C7)-eFluor 660 (eBioscience) at 1/200 overnight at 4°C, followed by donkey anti-rat IgG AF647 (Jackson ImmunoResearch) at 1/400 for 2 hours at 4°C. Stained bone sections on the films were sandwiched between the coverslip and glass slide using the modified Kawamoto's film method for improved resolution (18). Images were captured with an all-in-one fluorescence microscope BZ-X800 (Keyence). Fluorescence intensity and vessel diameter were analyzed using Keyence image analysis software.

Imaging of 2,2-thiodiethanol-cleared bone

Thick sections of bones were stained and cleared as described previously, with some modifications (19). Femurs were fixed in 4% PFA at 4°C for 24 hours, washed with PBS, and transferred into a 30% sucrose solution at 4°C overnight with constant shaking. Samples were cooled in dry ice-cooled hexane before being embedded in Super Cryoembedding Medium (SCEM) (Leica Microsystems) and were frozen using dry ice-cooled hexane. Frozen bones were trimmed using a tungsten carbide blade on a cryostat (Leica Biosystems) until the marrows were exposed. Cryofilm (Section-lab) was used to protect the surface of the marrow while trimming the other side of the bone. The marrow-exposed thick bone sections were washed in Tris-buffered saline (TBS) thrice to remove SCEM. Each sample was transferred to a cover glass attached to an iSpacer IS003 (SunJin Lab). Samples were blocked with 10% donkey serum in TBS with 0.05% Tween 20 (TBST) for 2 hours at room temperature and washed with TBST thrice before staining with anti-endomucin (V.7C7)-eFluor 660 (eBioscience) at 1/200 for 3 days at 4°C. Samples were washed five times with TBS and stained with donkey anti-rat IgG AF647 (Jackson ImmunoResearch) at 1/400 overnight at 4°C. After washing samples in TBS five times, serial optimal clearance was performed using 2,2-thiodiethanol (TDE) in TBS (Sigma–Aldrich) up to 70% instead of 100% to prevent quenching of the GFP signal (20). Cleared samples were mounted in 70% TDE with 0.1 M *N*-propyl gallate (Sigma–Aldrich). The refractive index of the mounting medium was 1.465, measured using a refractometer (Atago). Images were acquired using a Zeiss Lightsheet 7 microscope (Carl Zeiss) at 5× magnification. Three-dimensional (3D) images and videos were constructed using Imaris software.

Statistical analysis

Graphs were plotted and analyzed using GraphPad Prism 9.5 software. Data are expressed as means ± SD. Each data point represents an individual mouse. The Mann–Whitney *t*-test was used to compare two groups, while ordinary one-way analysis of variance was used to compare more than two groups. Statistical significances are represented as ns; not significant, $*P < .05$, $**P < .01$, and $***P < .001$. Some figures were created using BioRender.com.

Results

Malaria alters the lymphopoietic niche in the bone marrow

To examine the effect of uncomplicated malaria on the lymphopoietic niche in the bone marrow, we infected the mice with *Py*NL and analyzed *Cxcl12* and *Il7* gene expression in the bone marrow (Fig. 1A). We found that both *Cxcl12* and *Il7* significantly reduced in the bone marrow during uncomplicated malaria, but eventually returned to comparable levels as naïve controls on Day 30 post-infection when the mice completely recovered from the infection (Fig. 1B). To visualize CAR cells in the bone marrow, we examined the bone sections of CXCL12-GFP mice infected with *Py*NL by immunohistochemistry and 3D imaging of bones cleared by the TDE method. Consistently we found that CXCL12-GFP-expressing cells were reduced in the bone marrow (Fig. 1C and E). CAR cells are located at perivascular areas of vessels (8), and we noticed dilation of endomucin$^+$ sinusoidal vessels in the bone marrow during acute malaria (Fig. 1D).

Bone marrow CAR cells are affected by malaria

To further examine the effects of malaria on the CAR cell population, bone marrow populations were analyzed by flow cytometry (Fig. 2A). We found that CAR cells, defined as CD45$^-$ Ter119$^-$ CD31$^-$ Sca1$^-$ PDGFRβ$^+$ cells, significantly reduced in the bone marrow at acute infection (Fig. 2B). We also observed the same phenomenon in chronic malaria and acute severe malaria models infected with *Pcc* and *Pb*A, respectively (Fig. 2C and D). In contrast, there was a significant increase of a population of PDGFRβ$^+$ stromal cells with upregulated Sca1 expression in the bone marrow. Next, to determine whether Sca1 is upregulated on CAR cells, we infected CXCL12-GFP mice and examined the total population of CXCL12-GFP$^+$ PDGFRβ$^+$ cells. We found that CXCL12-GFP$^+$ PDGFRβ$^+$ CAR cells were reduced after infection and Sca1 expression increased in this population (Fig. 2E). Next, to examine the gene expression of typical CAR cell markers such as transcription factors *Foxc1*, *Ebf3*, and *Kitl* (encodes SCF) (21, 22), chemokine *Cxcl12* and cytokine *Il7* in this CXCL12$^+$ Sca1$^+$ PDGFRβ$^+$ population that arises during

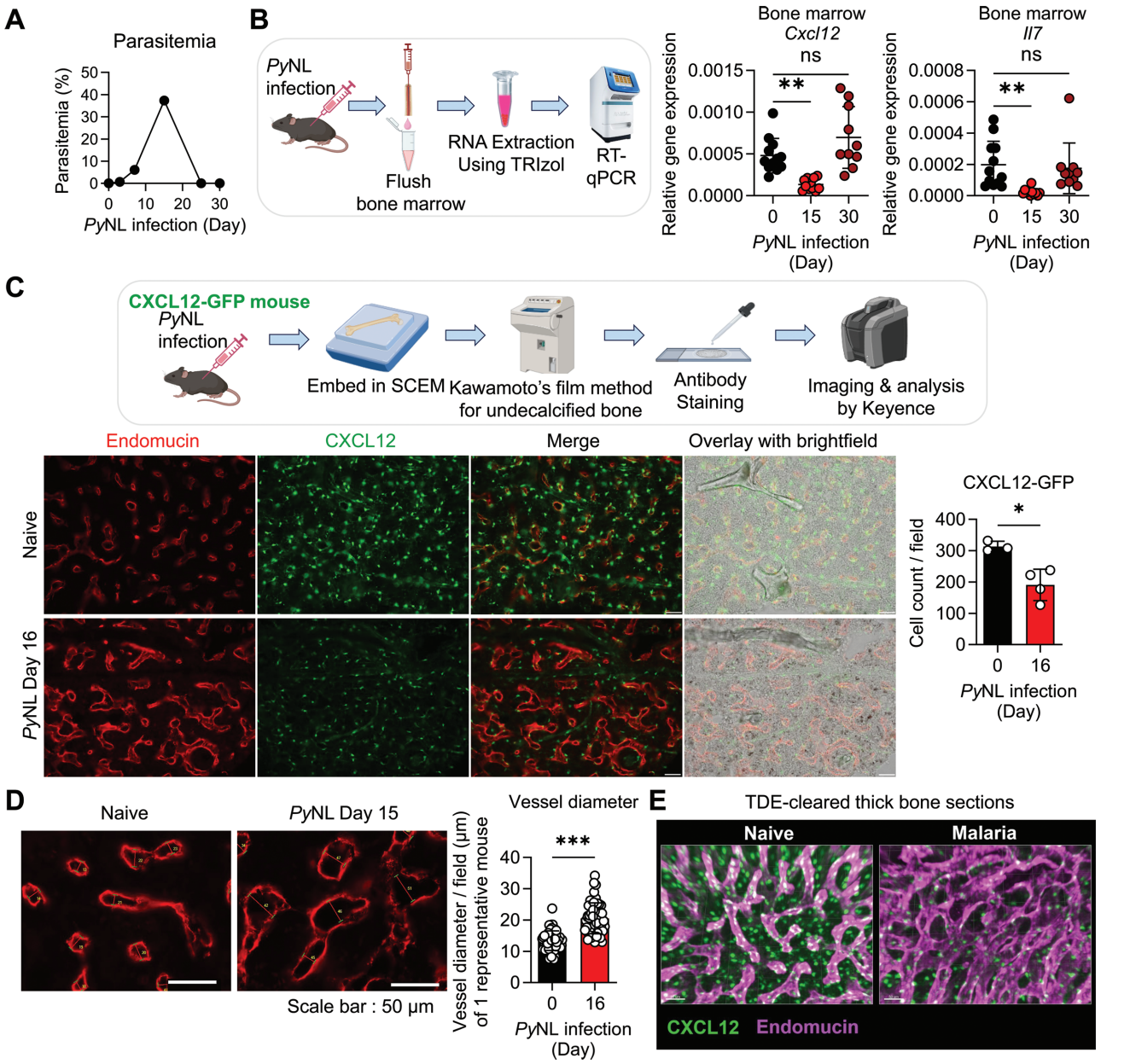

Figure 1. Acute malaria infection suppresses the bone marrow CXCL12 and IL-7 lymphocytic niche. (A) Parasitemia of *Py*NL infection. (B) Relative gene expression of *Cxcl12* and *Il7* from total bone marrow cells without RBC lysis from tibia of naive mice and *Py*NL-infected mice on Day 15 and Day 30. (C and D) Representative images of immunohistochemical analysis of femurs of naive ($n = 3$) and *Py*NL-infected CXCL12-GFP mice ($n = 4$) stained with endomucin (sinusoidal endothelial cells). Scale bar is 50 μm. Quantitative analysis of (C) average cell count of CAR cells per field in individual mouse, and (D) vessel diameter per field of a representative mouse. (E) Still image of video showing the 3D imaging of TDE-cleared bone from naïve and *Py*NL-infected CXCL12-GFP mice stained with endomucin. Scale bar is 50 μm. See Supplementary video.

malaria, we sorted CXCL12$^+$ Sca1$^-$ and CXCL12$^+$ Sca1$^+$ cells from naïve and *Py*NL-infected mice (Fig. 2F). We found that CXCL12$^+$ Sca1$^+$ cells from infected mice expressed higher *Foxc1* and *Kitl*, and comparable *Ebf3*, *Cxcl12*, and *Il7* to CXCL12$^+$ Sca1$^-$ CAR cells from naïve mice (Fig. 2G). This CXCL12$^+$ Sca1$^+$ cell population induced by malaria did not increase *Col3a1* expression, indicating that they are not fibrotic CAR cells (Fig. 2G). This suggests that although CXCL12$^+$ Sca1$^-$ CAR cells are reduced during infection, malaria induces the expansion of a CXCL12$^+$ Sca1$^+$ cell population that expresses CAR cell markers.

Acute malaria infection induces expansion of HSCs but leads to bias in the differentiation of multipotent progenitors

Since CAR cells play important roles in regulating hematopoiesis and lymphopoiesis in the bone marrow, we, therefore,

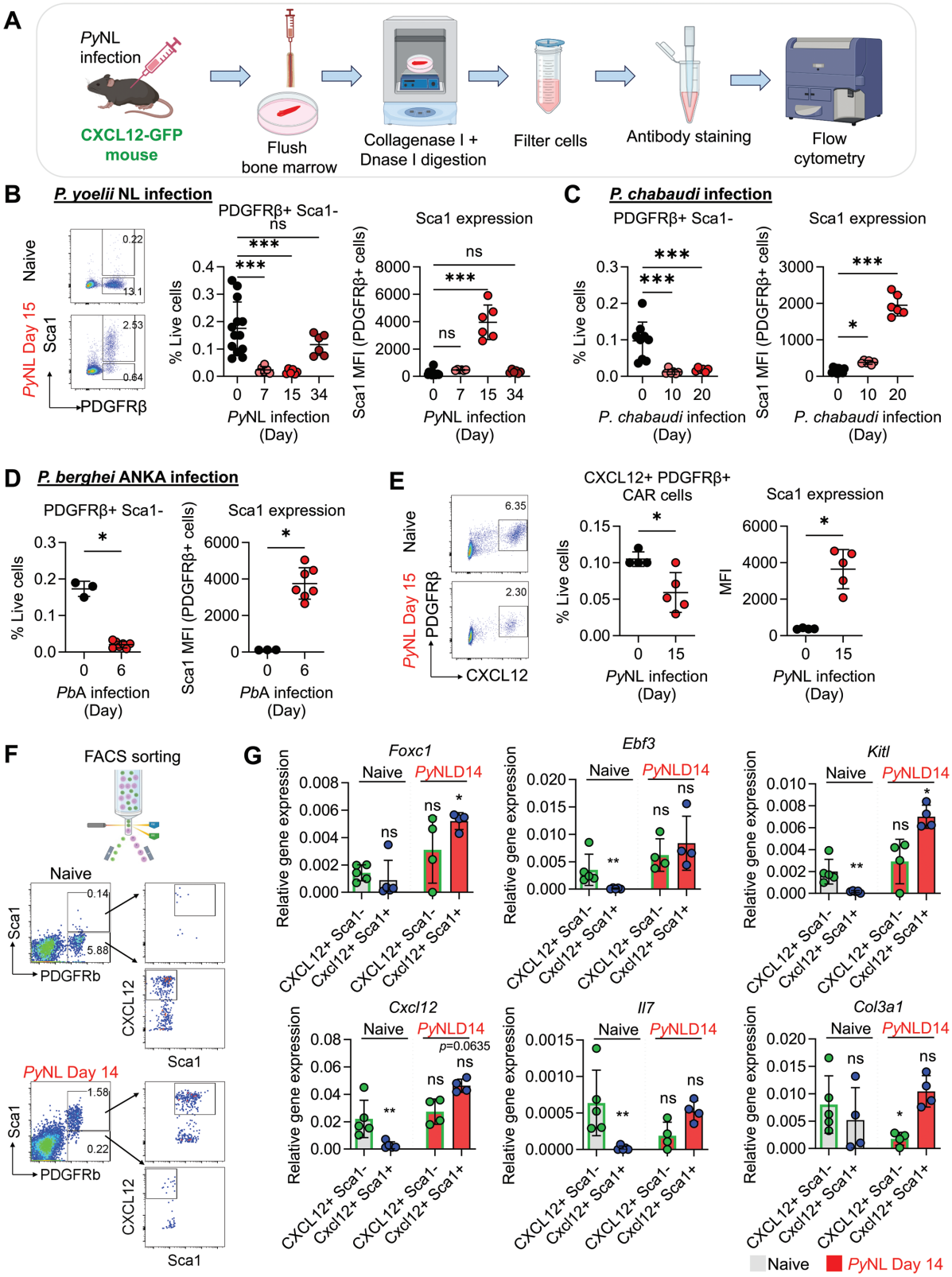

Figure 2. Acute malaria infection induces Sca1 upregulation on CAR cells. (A) Schematic diagram of experimental protocol for (B–E). (B–D) Flow cytometry analysis of the bone marrow CD45⁻ Ter119⁻ CD31⁻ PDGFRβ⁺ Sca1⁻ CAR cell population and mean fluorescence intensity (MFI) of Sca1 on the CD45⁻ Ter119⁻ CD31⁻ PDGFRβ⁺ population in mice infected with (B) *Py*NL infection, (C) *P. chabaudi* infection, (D) *P. berghei ANKA* infection. (E) Flow cytometry analysis of the bone marrow CD45⁻ Ter119⁻ CD31⁻ CXCL12-GFP⁺ PDGFRβ⁺ CAR cell population and Sca1 expression (MFI) on Day 15 *Py*NL infection. (F) Representative flow cytometry plots of cell populations sorted by flow cytometry for analysis of gene expressions. Live cells were gated from CD45⁻ Ter119⁻ CD31⁻ PDGFRβ⁺ and further sorted as Sca1⁻ CXCL12⁺ cells or Sca1⁺ CXCL12⁺ cells. (G) Relative gene expression of *Foxc1, Ebf3, Kitl, Cxcl12*, *Il7*, and *Col3a1* in Sca1⁻ CXCL12⁺ and Sca1⁺ CXCL12 cell populations sorted from naïve mice and *Py*NL-infected mice on Day 14. **P* < .05, ***P* < .01; ns, not significant by Mann–Whitney *t*-test comparing each group with the naïve CXCL12⁺ Sca1⁻ control group.

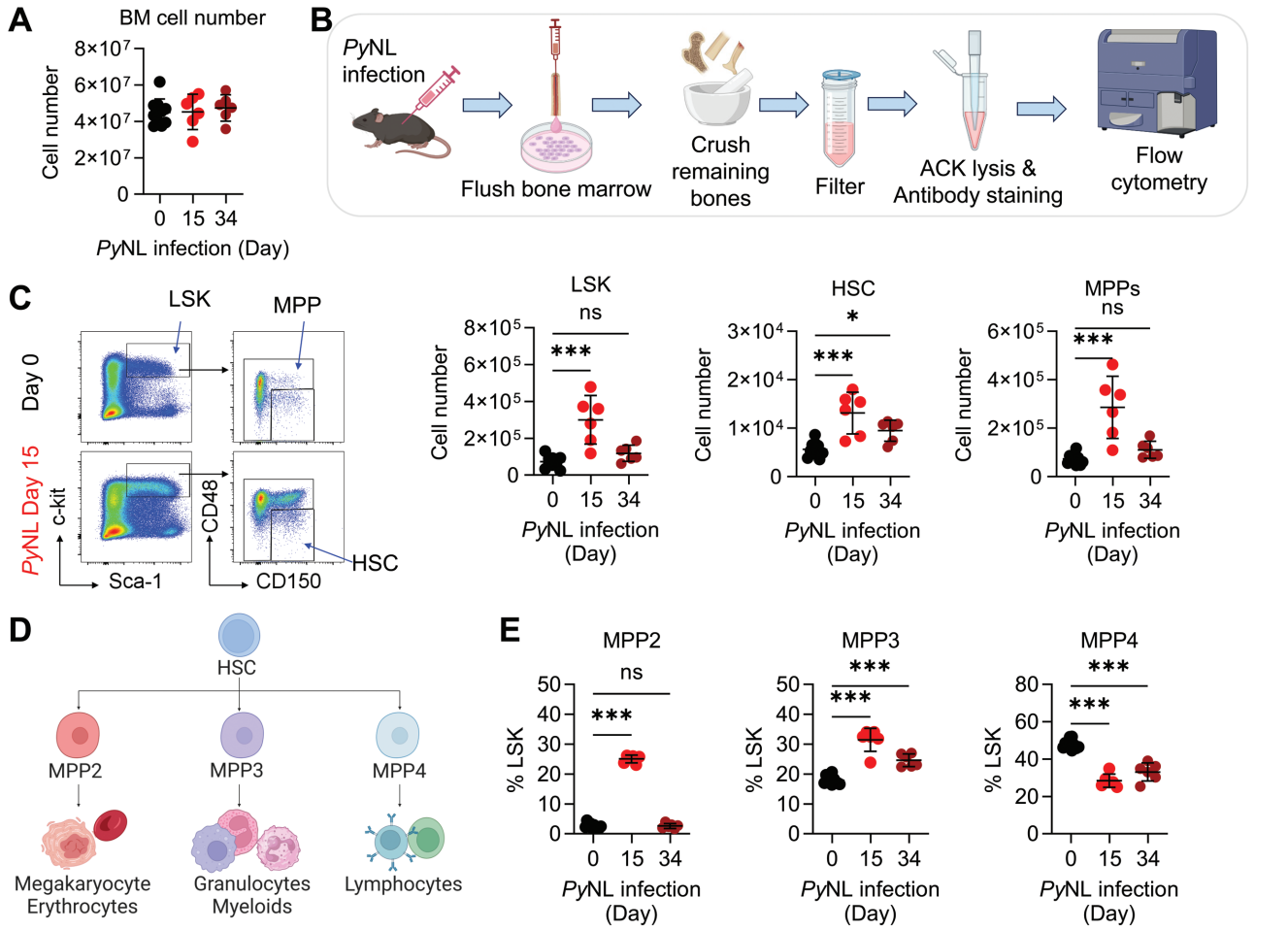

Figure 3. Acute malaria infection induces expansion of HSCs but leads to bias in the differentiation of multipotent progenitors. (A) Total cell numbers in bone marrow from two femurs and two tibias per mouse after ACK lysis. (B) Schematic diagram of experimental protocol for (C–L). (C) Cell numbers of Lin⁻ Sca1⁺ c-Kit⁺ (LSK), CD150⁺ CD48⁻ hematopoietic stem cell (HSC), and multipotent progenitors (MPPs) in the bone marrow of naive, Day 15 and Day 34 post-infection with *Py*NL. (D) Schematic diagram of HSC differentiation and MPP lineage commitment in the bone marrow. (E) Percentage of MPP2 (Lin⁻ Kit⁺ Sca1⁺ Flt3⁻ CD150⁺ CD48⁺), MPP3 (Lin⁻ Kit⁺ Sca1⁺ Flt3⁻ CD150⁻ CD48⁺), and MPP4 (Lin⁻ Kit⁺ Sca1⁺ Flt3⁺ CD48⁺) cell populations within the LSK population.

examined the effects of malaria on the development of bone marrow cell populations. The total cell number in the bone marrow did not change during the course of infection (Fig. 3A). However, Lin⁻ Sca1⁺ c-kit⁺ (LSK), HSC, and MPP populations significantly increased during acute infection, indicating enhanced hematopoiesis (Fig. 3B–D). Next, we analyzed the subsets of MPP populations with developmental potential to become erythrocyte/megakaryocyte (MPP2), myeloid/granulocyte (MPP3), and lymphocyte (MPP4) lineages (23). We found that the expansion of MPP populations was biased toward MPP2 and MPP3 populations, while the MPP4 population was restricted (Fig. 3E).

Consistent with the increase of the MPP2 population, using Ter119 and CD44 markers to distinguish five stages of erythroid development (24), we found that all erythroid progenitors were increased in the bone marrow during acute *Py*NL infection (Fig. 4A), suggesting that *Py*NL infection does not suppress erythropoiesis in the bone marrow despite malaria-induced hemolytic anemia in the blood. We further examined the population downstream of MPP3, which are the myeloid cells in the bone marrow. Surprisingly total CD11b⁺ cells and neutrophil populations slightly decreased in the bone marrow, whereas the Ly6C⁺ Ly6G⁻ monocyte population did not change during malaria infection (Fig. 4B). Previous study showed that CD11b⁺ Gr1⁺ neutrophils increased in the spleen during acute *Py*NL infection (25), suggesting that the slight decline of the CD11b⁺ population in the bone marrow is likely due to their mobilization to the periphery. These data indicate that acute malaria infection enhances hematopoiesis but induces bias in the lineage development of multipotent progenitor cells.

Acute malaria infection restricts B lymphopoiesis and retention of mature B cell populations in the bone marrow

Next, we examined the development of B cell progenitors downstream of the MPP4 population. Consistent with the reduction of the MPP4 population in the bone marrow (Fig. 3E), we observed the reduction of the Flt3⁺ IL-7R⁺ CLP population (Fig. 5A). Furthermore, Sca1 and cKit expression was

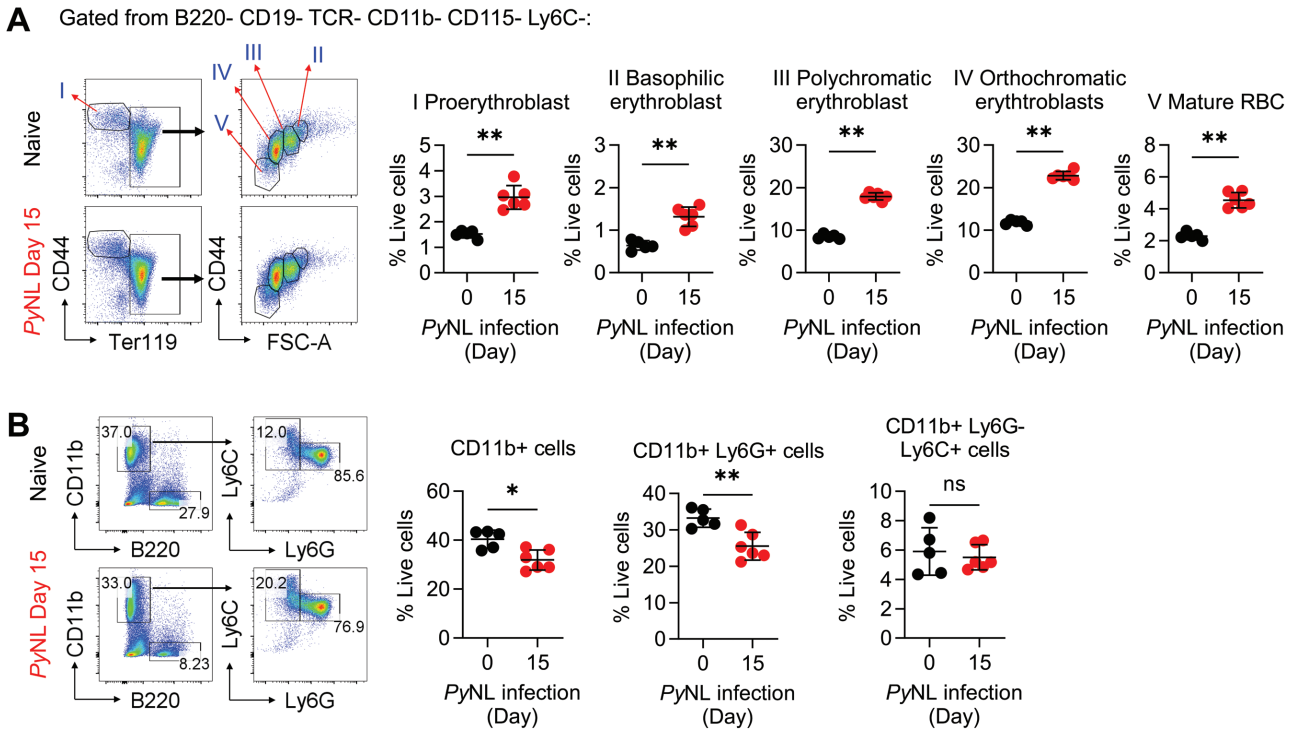

Figure 4. Acute malaria infection increases erythropoiesis and sustains myelopoiesis in the bone marrow. (A) Representative FACS plots and populations of proerythroblasts, basophilic erythroblasts, polychromatic erythroblasts, orthochromatic erythroblasts, and mature erythrocytes in the bone marrow of naïve and *Py*NL-infected mice on Day 15. (B) Representative FACS plots and populations of total CD11b$^+$ myeloid cells, CD11b$^+$ Ly6G$^+$ neutrophils, and CD11b$^+$ Ly6G$^-$ Ly6C$^+$ monocytes in the bone marrow of naïve and *Py*NL-infected mice on Day 15.

increased on the CLP population (Fig. 5B). Previously it was shown that IL-7R$^+$ cKit^{hi} progenitors that arose during *P. chabaudi* infection exhibited myeloid–lymphoid bipotential *in vitro* and mainly generated myeloid cells *in vivo* (26). We further investigated B cell development downstream of the CLP and found that pre-B cell, immature B cell and mature B cell populations were significantly reduced at peak infection (Fig. 5C and D), but eventually returned to the steady-state level after recovery from infection on Day 34 (Fig. 5E). Bone marrow not only serves as a niche for early B cell development but also harbors mature long-lived plasma cells. Plasma cells are readily detected in the bone marrow in the steady state, and they are mostly IgA$^+$ and originated from the gut mucosa (27–29). We found that the bone marrow IgA$^+$ antibody-secreting cells (ASCs) were greatly reduced, whereas IgG$^+$ ASCs significantly increased (Fig. 5F). To distinguish preexisting plasma cells and newly formed plasmablasts during infection, flow cytometry analysis was performed by separating TACI$^+$ CD138$^+$ cells into B220$^-$ CD19$^-$ plasma cells and B220$^+$ CD19$^+$ plasmablasts (30, 31). We found that plasma-cell populations were greatly reduced in the bone marrow at peak infection, despite the increase of newly formed plasmablasts (Fig. 5G). Collectively, we demonstrated the disruption of the B lymphocytic niche in the bone marrow that supports B cell development and plasma-cell retention during malaria infection.

Despite the reduction of all B lymphocyte subsets in the bone marrow, we did not observe a reduction of T lymphocytes in the bone marrow, but rather a significant increase of CD4$^+$ T cells and CD8$^+$ NKT cells (Fig. 6A). Further analysis of the activation of CD4$^+$ and CD8$^+$ T cells revealed that most of the CD4$^+$ T cells in the bone marrow were CD44$^+$ effector T cells during malaria infection. About 30% of these CD44$^+$ CD4$^+$ T cells also express CD49d in infected mice (Fig. 6A), which was previously defined as antigen-specific Th1 effector T cells (32). Consistently, the populations of IFNγ-producing CD4$^+$ T cells and CD8$^+$ T cells increased significantly in the bone marrow (Fig. 6B). These data indicate that T cell development was not suppressed, and T cells contribute to Th1 immune response within the bone marrow during malaria infection.

IFNγ is responsible for the upregulation of Sca1 on CAR cells but not for the reduction of CAR cell and B cell populations in the bone marrow

The induction of IFNγ in *P. berghei* ANKA, *Ehclichia muris*, or *Mycobacterium avium* was shown to suppress HSC quiescence to promote myeloid-biased hematopoiesis (14, 33, 34). Moreover, the acquisition of a myeloid differentiation potential of atypical CLPs induced by *P. chabaudii* infection was also IFNγ dependent (26). IFNγ is upregulated in the bone marrow during *Py*NL infection (Fig. 7A). To examine whether IFNγ affects the CAR cell population during malaria, we crossed IFNγR-knockout mice with CXCL12-GFP mice and infected them with *Py*NL. We found that the reduction of the CAR cell population during acute infection is IFNγR-independent (Fig. 7B). However, Sca1 upregulation on CAR cells is IFNγR-dependent (Fig. 7C). Although the reduction of the CLP population is also partially IFNγR-dependent (Fig. 7D), the reduction of Pro-B cell, Pre-B cell, immature B cell, mature B cell and

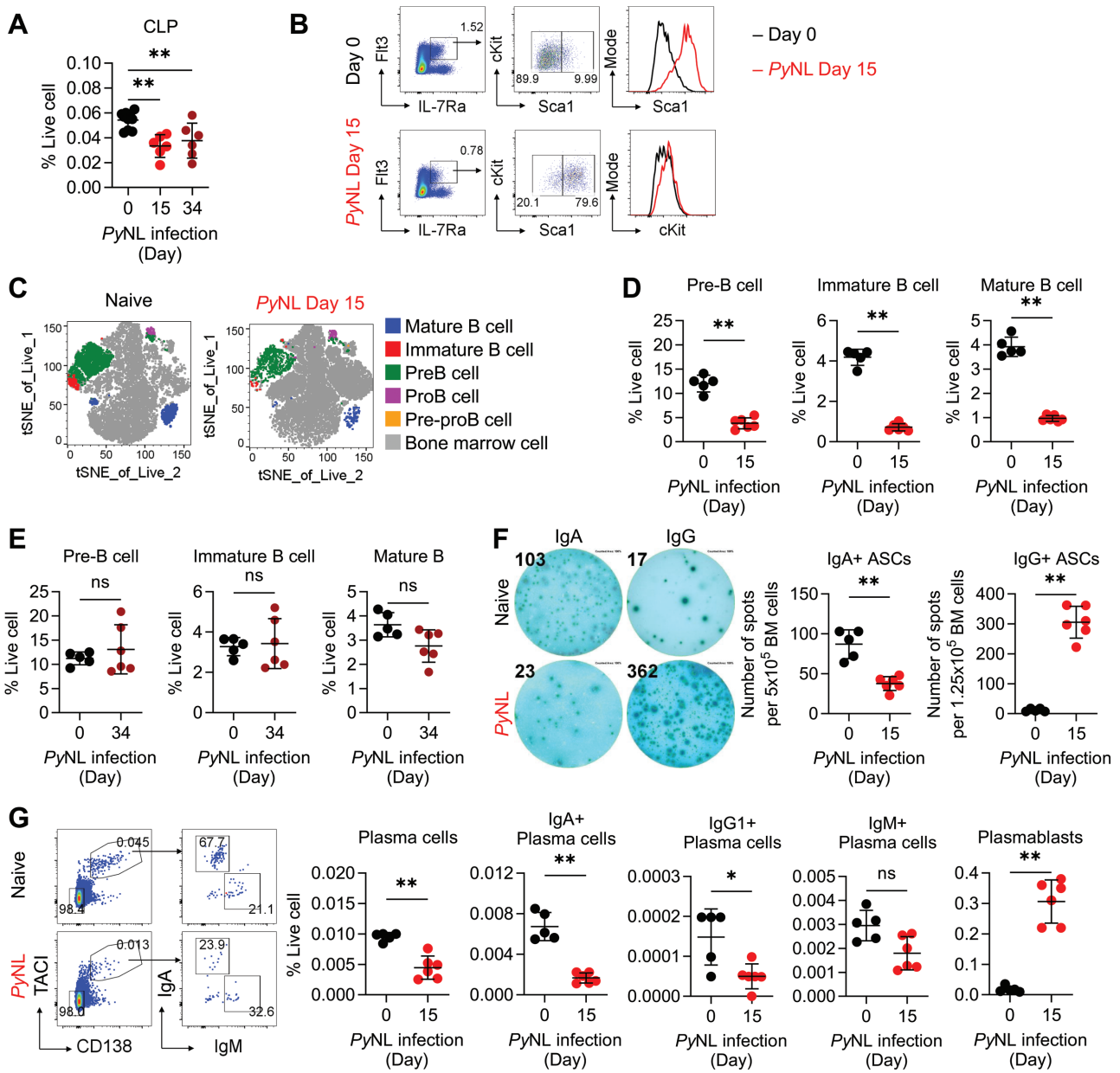

Figure 5. Acute malaria infection restricts B lymphopoiesis and retention of mature B cell populations in the bone marrow. (A) Percentage of the CLP (Lin$^-$ Kit$^{+/lo}$ Sca1$^{+/lo}$ Flt3$^+$ IL7Ra$^+$) cell population within total live cells in the bone marrow analyzed by flow cytometry. (B) Representative FACS plots of CLP and histogram plots of Sca1 and cKit expression on CLP populations from naïve and *Py*NL-infected mice on Day 15. (C) Representative t-SNE plot of B cell subsets in the bone marrow of naïve mouse and *Py*NL-infected mice on Day 15 analyzed by flow cytometry. (D, E) Pre-B cell (CD19$^+$ B220^{lo} cKit$^-$ IgD$^-$ IgM$^-$ CD24$^+$), immature B cell (CD19$^+$ B220^{lo} cKit$^-$ IgD$^-$ IgM$^+$ CD24$^+$), mature B cell (CD19$^+$ B220$^+$ cKit$^-$ IgD$^+$) populations in the bone marrow of naïve and *Py*NL-infected mice on (D) Day 15 and (E) Day 34. (F) Representative images of ELISPOT wells and spot counts representing IgA$^+$ and IgG$^+$ ASCs in the bone marrow of naïve and *Py*NL-infected mice on Day 15. (G) Representative FACS plots gated from CD19$^-$ B220$^-$ cells and percentage of total plasma cells (CD19$^-$ B220$^-$ TACI$^+$ CD138$^+$), IgA$^+$, IgG1$^+$, IgM$^+$ plasma cells and total plasmablasts (CD19$^+$ B220$^+$ TACI$^+$ CD138$^+$) in the bone marrow of naïve and *Py*NL-infected mice.

plasma cell populations in the bone marrow were not IFNγ-dependent (Fig. 7E and F). The lack of effects of IFNγ on B cell subsets could possibly be explained by a previous study using intravital live imaging to show that IFNγ injection into mice led to increased distance between HSCs and CAR cells in the HSC niche; however, this effect was not observed between CAR cells and CD19$^+$ B cells (35). We observed that the *Py*NL-induced increase of CD8$^+$ NKT cells and CD4$^+$ T cells in the bone marrow is abolished in IFNγR-deficient mice (Fig. 7G), suggesting that these cells are not responsible for the depletion of CAR cell and B cell populations in the bone marrow.

Discussion

Hematopoietic stem cells possess the ability of self-renewal and retain the multipotency function to constantly replenish

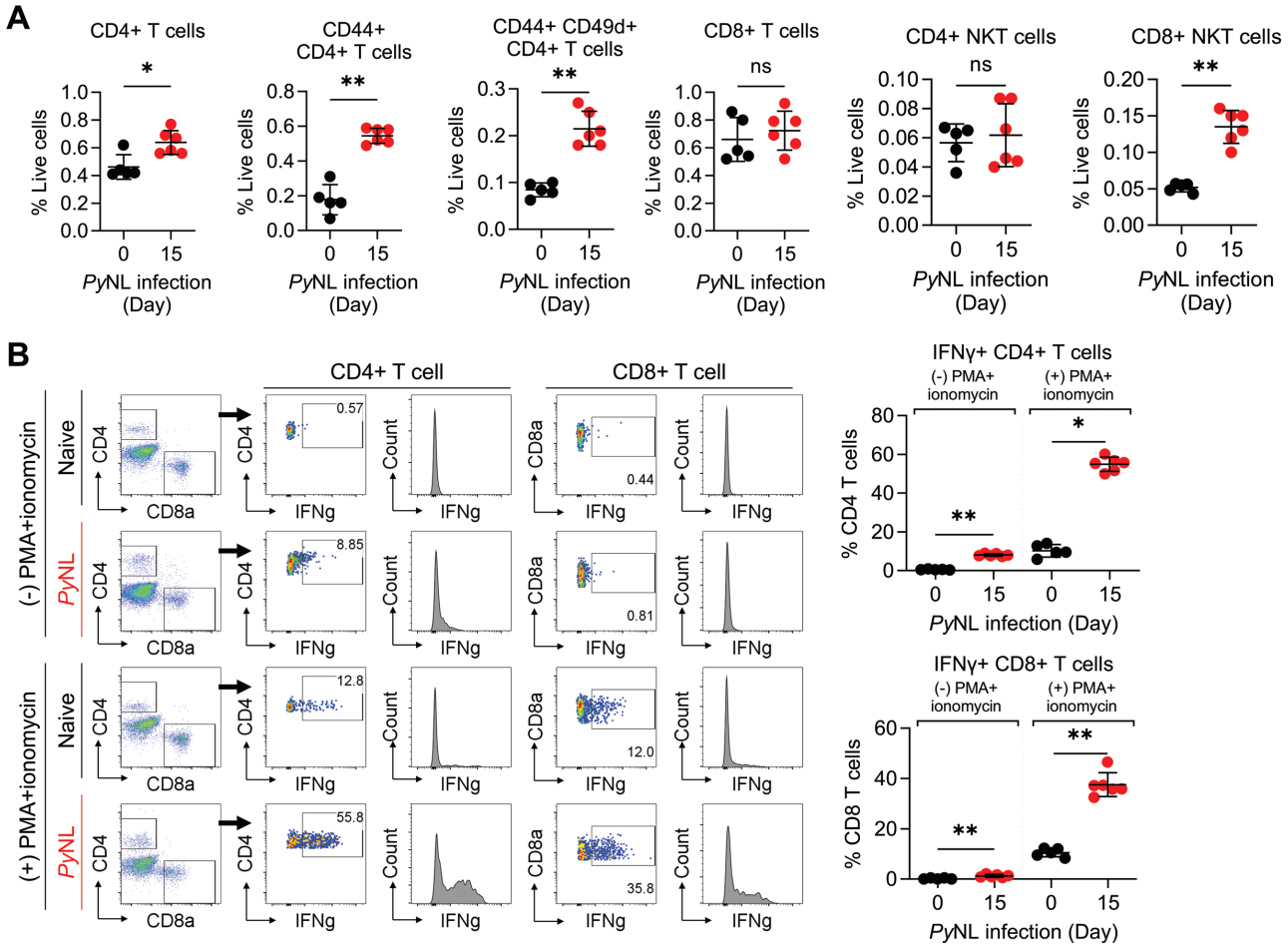

Figure 6. T cells in the bone marrow exhibit a Th1 response during acute malaria infection. (A) CD4⁺ T cells, CD44⁺ CD4⁺ T cells, CD44⁺ CD49d⁺ CD4⁺ T cells, CD8⁺ T cells, CD4⁺ NKT cells, and CD8⁺ NKT cells in the bone marrow on Day 15 *Py*NL infection. (B) IFNγ-producing CD4⁺ T cells and CD8⁺ T cells in the bone marrow of naïve and Day 15 *Py*NL-infected mice.

blood cells. The survival and development of lineage-committed HSPC progenies rely on instructive signals from other cells in the bone marrow microenvironment that make up the HSC niche (36). In this study, we demonstrated that acute malaria infection depletes the CAR cell population, which is the major source of CXCL12 and IL-7 for lymphopoietic niche, and this leads to the suppression of early B cell development and reduction of mature preexisting plasma cells in the bone marrow, despite the increase of hematopoiesis. We found that malaria induces the emergence of Sca1⁺ CAR cells during acute infection. PDGFRα⁺ Sca1⁺ cells (PαS) are multipotent mesenchymal progenitors that can give rise to CAR cells, but they do not express CXCL12 (37), indicating that the malaria-induced Sca1⁺ CAR cells are not PαS cells. A recent study showed the upregulation of Sca1 on Runx1/2-deficient CAR cells which exhibit a fibrotic phenotype and lead to the depletion of total bone marrow hematopoietic cells, despite the increased number of CAR cells in the bone marrow of the mutant mice (38). We noticed that the Sca1⁺ CAR cell population greatly increased at peak infection on Day 15 following the reduction of Sca1⁻ CAR cells at the early phase of infection on Day 7. Further studies are required to clarify whether the malaria-induced Sca1⁺ CAR cell population is a progeny arising from PαS cells or is a population of altered CAR cells that may be required to repopulate CAR cells during the recovery phase of malaria infection. Gene expression analysis of sorted Sca1+ CAR cells showed that they express CAR cell markers including *Foxc1*, *Ebf1*, *Cxcl12*, *Kitl*, and *Il7*, although they do not express the *Col3a1* fibrotic gene. The loss of osteoblasts during acute infection (13), possibly further restricts the availability of IL-7 to support the B lymphocytic niche. Although the increase of Sca1 expression in CAR cells is mediated by IFNγ, the reduction of CAR cells and B cell subsets in the bone marrow were IFNγ-independent during malaria infection. Nevertheless, CAR cell and B cell populations were restored after recovery from the infection.

The effects of malaria on the bone marrow microenvironment share some similarities and differences with other bacteria or virus infections (39). Total bone marrow cells and CD150⁺ HSCs are depleted by bacteria and virus infections (40, 41). However, we found that these populations expanded during acute *Py*NL infection in this study, and in severe *Pb*ANKA infection reported previously (14). The reduction of CAR cells did not deplete HSCs in the bone marrow during malaria, which is consistent with a previous finding that even up to 70% deletion of CXCL12 in CAR

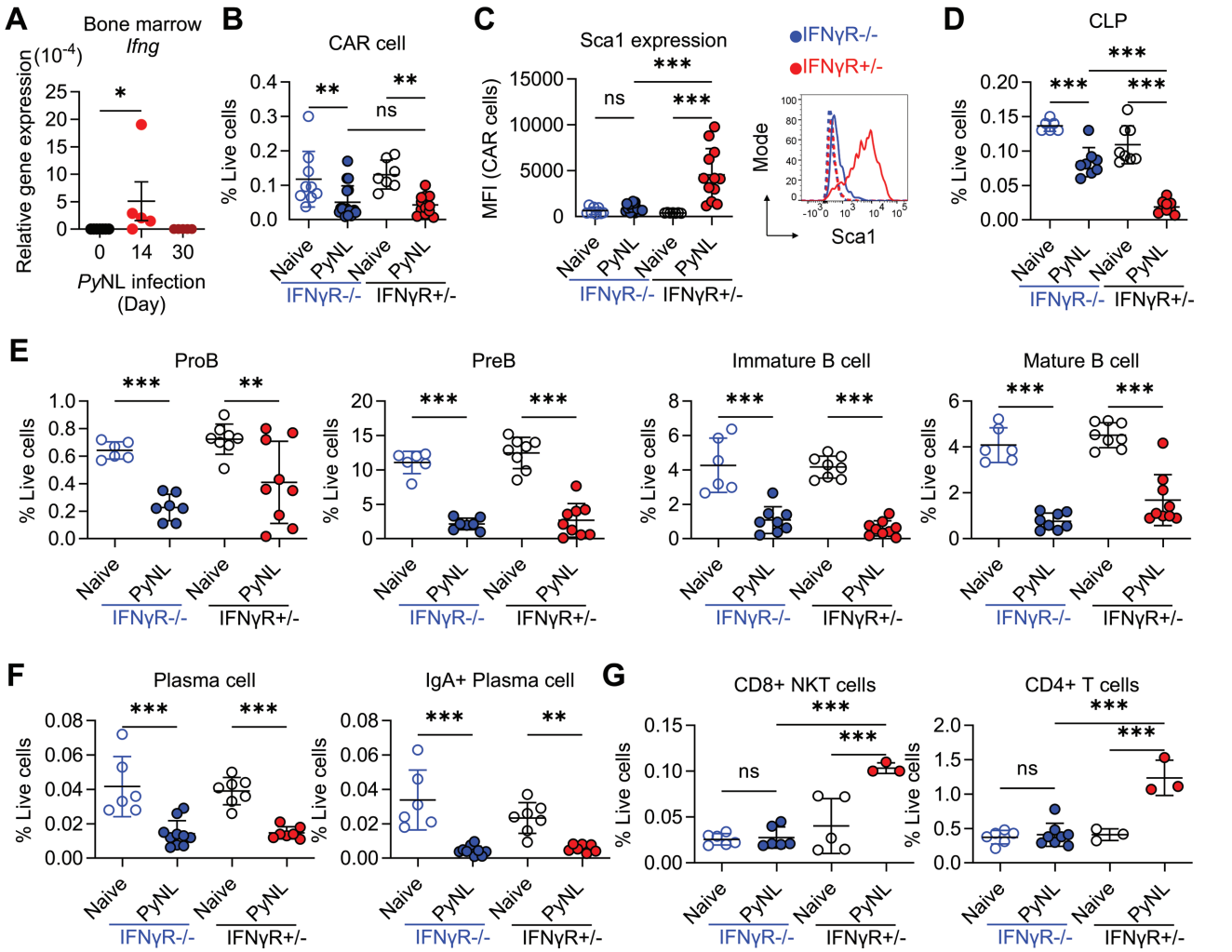

Figure 7. IFNγ is responsible for Sca1 upregulation on CAR cells but not responsible for the reduction of CAR cell and B cell populations in the bone marrow. (A) Relative gene expression of *Ifng* in the bone marrow of naive and *Py*NL-infected mice on Day 14 and Day 30. (B) Percentage of CAR cell populations in the bone marrow of naive and *Py*NL-infected mice on Day 21 from IFNγR$^{-/-}$ and IFNγR$^{+/-}$ mice. (C) Mean fluorescence intensity (MFI) of Sca1 expression on CAR cells of naïve and *Py*NL-infected mice on Day 21 from IFNγR$^{-/-}$ and IFNγR$^{+/-}$ mice. Dotted lines represent CAR cells from naïve mice. Solid lines represent CAR cells from *Py*NL-infected mice. (D) The CLP population in the bone marrow of naïve and *Py*NL-infected mice on Day 21 from IFNγR$^{-/-}$ and IFNγR$^{+/-}$ mice. (E) Pro-B cell, pre-B cell, immature B cell, and mature B cell populations in the bone marrow of naïve and *Py*NL-infected mice on Day 21 from IFNγR$^{-/-}$ and IFNγR$^{+/-}$ mice. (F) Populations of plasma cells in the bone marrow of naïve and *Py*NL-infected mice on Day 22 from IFNγR$^{-/-}$ and IFNγR$^{+/-}$ mice. (G) CD8$^+$ NKT cells and CD4$^+$ T cells in the bone marrow of naïve and *Py*NL-infected mice on Day 22 from IFNγR$^{-/-}$ and IFNγR$^{+/-}$ mice.

cells is sufficient to maintain normal numbers of HSCs in Ebf3-CreERT2; CXCL12f/$^-$ mice (42). In bacterial infection, increased HSC mobilization from the bone marrow to the spleen is mediated by granulocyte colony-stimulating factor (G-CSF) dependent on NOD1 and TLR4 in radio-resistant cells (40), and the suppression of lymphopoiesis in the bone marrow is mediated by G-CSF-induced depletion of IL-7-producing osteoblasts independent of TLR signaling (43). Although G-CSF treatment was shown to suppress the expression of B cell trophic factors including CXCL12, IL-7, and stem cell factor (SCF) from CAR cells, instead it leads to the expansion of CAR cell populations and promotes osteogenic lineage commitment (44). In contrast, we found that CAR cell populations were reduced during malaria infection, whereas the gene expression of CXCL12, IL-7, and SCF were not suppressed in CAR cells sorted from malaria-infected mice. In LCMV virus infection, CAR cells are directly infected by the virus, and that triggers CD8$^+$ T cell-mediated killing of CAR cells (41). Unlike viral infection, *Plasmodium* parasites do not infect cells other than red blood cells, and we did not find an increase infiltration of CD8$^+$ T cells into the bone marrow of *Py*NL-infected mice at peak infection. Moreover, the IFNγ-mediated increase of CD8$^+$ NKT cells was not responsible for the depletion of CAR cells observed in IFNγR-deficient mice. The mechanism of how malaria causes the depletion of the CAR cell population requires further investigation.

Mature B cells migrate to peripheral lymphoid organs and differentiate into plasma cells upon antigen activation. These terminally differentiated plasma cells home to the bone marrow using the CXCL12 chemokine and receive signals from several other cell types in the bone marrow niche for

survival (12, 45). The decline in the CAR cell populations and increased vasodilation during malaria suggest that the depletion of B cell populations in the bone marrow may be a result of increased B cell mobilization. Peripheral B cells form germinal centers to produce malaria-specific memory B cells and plasma cells in the spleen (46). Immunization or commensal bacteria in the gut can give rise to long-lived plasma cells in the bone marrow to protect from systemic infection (27, 28). The depletion of plasma cells in the bone marrow may increase the risk of other infections. In fact, co-infections are not uncommon among malaria patients in endemic regions (47). Long-lived plasma cells promptly produce antibodies upon antigen encounter to prevent disease progression and therefore are important for long-lasting humoral immunity against infection. Evidence in a malaria-endemic region in Mali showed that malaria was associated with accelerated declines in antibodies specific for tetanus, measles, and hepatitis B in vaccinated children (3). Further investigations in murine malaria models demonstrated the depletion of antibodies against previous influenza vaccination and influenza-specific ASCs after malaria infection (3), suggesting that malaria may compromise preexisting vaccine responses because of the depletion of bone marrow plasma cells. In several vaccine clinical trials, reduced antibody responses against vaccinations were shown to be associated with the frequency of repeated malaria infections or concomitant infection during vaccination because of immune tolerance as one of the evasion strategies of the *Plasmodium* parasite (48). It is therefore crucial to understand the factors that contribute to the suppression of vaccine responses to improve vaccine design and immunization schedules.

Interestingly, despite the potential increased susceptibility to other infections, malaria exerts certain protective effects on autoimmune diseases such as systemic lupus erythematosus via modulation of B cells (49). A recent study further suggests that the alteration of the bone marrow microenvironment by malaria exhibits a long-lasting protective effect against lethal autoimmune nephritis; however, it is independent of the chronic retention of the *Plasmodium* byproduct hemozoin in the bone marrow (50). Our previous study showed that hemozoin exhibits immunomodulatory effects (51), and instead contributes to malaria-induced inflammation in the bone (13). This suggests that the effects of malaria infection on the bone marrow may leave a chronic impact on the host immunity and a vaccination boost should be considered after malaria infection if antibody titers to previous vaccinations rapidly declined, in order to remain protected against preventable infections.

Repeated malaria infections give rise to partial immunity that protects from symptomatic malaria. Asymptomatic malaria was recently found to be prevalent in malaria-endemic regions, which contributed to under-reported cases (52). Asymptomatic malaria may potentially affect hematopoiesis and host immunity if it remains undiagnosed and untreated. *Plasmodium vivax* preferentially infects immature red blood cells and hides within the bone marrow while remaining undetectable in the peripheral blood, making it a challenge for diagnosis and elimination (53). Our study showed that most bone marrow populations recovered following complete clearance of parasites, suggesting the necessity to diagnose and treat asymptomatic malaria cases to prevent immune dysregulation and compromised immune responses to vaccinations.

Acknowledgements

We thank Ms Kayoko Suenaga (Carl Zeiss) for the image acquisition for 3D bone marrow imaging using a Zeiss Lightsheet 7 microscope.

Author contributions

M.S.J.L. conceptualized, performed experiments, analyzed data, and wrote the manuscript. J.M.-D. performed 3D microscope imaging analysis, performed qPCR, and assisted in some experiments. C.D.R.Z. performed some experiments and mouse maintenance. S.U. provided advice on immunohistochemistry staining and the 3D bone marrow staining and clearance method. Y.O. provided experiment guidance and scientific advice. T.N. provided CXCL12-GFP mice and scientific advice. A.I. provided experiment guidance and scientific advice. K.J.I. provided reagents and scientific advice. C.C. supervised the project and provided funding. All authors read, edited, and approved the final version of the manuscript.

Conflict of interest statement. None declared.

Funding

This study was supported by the Japan Society for the Promotion of Science (JSPS) KAKENHI grant numbers 20K16234 and 22K15448 (to M.S.J.L.), and the Mochida Memorial Foundation for Medical and Pharmaceutical Research (to M.S.J.L.), the Japan Science and Technology Agency JST-CREST program (to C.C. and K.J.I.), JST-CREST Young Challenge Program (to M.S.J.L.), AMED Strategic Center of Biomedical Advanced Vaccine Research and Development for Preparedness and Response (SCARDA) (JP223fa627001 and 223fa727001) (to C.C. and K.J.I.), the International Joint Usage/Research Center grant, and Mitsubishi UFJ vaccine development grant of the Institute of Medical Science, University of Tokyo.

Data availability

The data supporting the results of this study are available from the corresponding authors upon reasonable request.

References

1. World Health Organization. *World Malaria Report 2022*. Geneva, Switzerland: World Health Organization, 2022.
2. Rénia L, Goh YS. Malaria parasites: The great escape. *Front Immunol* 2016;**7**:1–14.
3. Banga S, Coursen JD, Portugal S, *et al*. Impact of acute malaria on pre-existing antibodies to viral and vaccine antigens in mice and humans. *PLoS One* 2015;**10**:e0125090–15. https://doi.org/10.1371/journal.pone.0125090
4. Hoshiba T, Chen G, Endo C, *et al*. Decellularized extracellular matrix as an *in vitro* model to study the comprehensive roles of the ECM in stem cell differentiation. *Stem Cells Int* 2016;**2016**:1–10.
5. Lee MSJ, Coban C. Unforeseen pathologies caused by malaria. *Int Immunol* 2018;**30**:121–9. https://doi.org/10.1093/intimm/dxx076
6. Coban C, Lee MSJ, Ishii KJ. Tissue-specific immunopathology during malaria infection. *Nat Rev Immunol* 2018;**18**:266–78. https://doi.org/10.1038/nri.2017.138
7. Brancucci NMB, Gerdt JP, Wang CQ, *et al*. Lysophosphatidylcholine regulates sexual stage differentiation in the human malaria parasite *Plasmodium falciparum*. *Cell* 2017;**171**:1532–1544.e15.
8. Sugiyama T, Omatsu Y, Nagasawa T. Niches for hematopoietic stem cells and immune cell progenitors. *Int Immunol* 2018;**31**:5–11.

9. Omatsu Y. Cellular niches for hematopoietic stem cells in bone marrow under normal and malignant conditions. *Inflamm Regen* 2023;**43**:15. https://doi.org/10.1186/s41232-023-00267-5
10. Cordeiro Gomes A, Hara T, Lim VY, *et al*. Hematopoietic stem cell niches produce lineage-instructive signals to control multipotent progenitor differentiation. *Immunity* 2016;**45**:1219–31. https://doi.org/10.1016/j.immuni.2016.11.004
11. Nagasawa T. Microenvironmental niches in the bone marrow required for B-cell development. *Nat Rev Immunol* 2006;**6**:107–16. https://doi.org/10.1038/nri1780
12. Tokoyoda K, Egawa T, Sugiyama T, *et al*. Cellular niches controlling B lymphocyte behavior within bone marrow during development. *Immunity* 2004;**20**:707–18.
13. Lee MSJ, Maruyama K, Fujita Y, *et al*. *Plasmodium* products persist in the bone marrow and promote chronic bone loss. *Sci Immunol* 2017;**2**:eaam8093.
14. Haltalli MLR, Watcham S, Wilson NK, *et al*. Manipulating niche composition limits damage to haematopoietic stem cells during *Plasmodium* infection. *Nat Cell Biol* 2020;**22**:1399–410. https://doi.org/10.1038/s41556-020-00601-w
15. Ding L, Morrison SJ. Haematopoietic stem cells and early lymphoid progenitors occupy distinct bone marrow niches. *Nature* 2013;**495**:231–5. https://doi.org/10.1038/nature11885
16. Greenbaum A, Hsu YMS, Day RB, *et al*. CXCL12 in early mesenchymal progenitors is required for haematopoietic stem-cell maintenance. *Nature* 2013;**495**:227–30. https://doi.org/10.1038/nature11926
17. Ara T, Tokoyoda K, Sugiyama T, *et al*. Long-term hematopoietic stem cells require stromal cell-derived factor-1 for colonizing bone marrow during ontogeny. *Immunity* 2003;**19**:257–67. https://doi.org/10.1016/s1074-7613(03)00201-2
18. Morodomi Y, Kanaji S, Won E, *et al*. Modified application of Kawamoto's film method for super-resolution imaging of megakaryocytes in undecalcified bone marrow. *Res Pract Thromb Haemost* 2020;**4**:86–91. https://doi.org/10.1002/rth2.12276
19. Coutu DL, Kokkaliaris KD, Kunz L, *et al*. Multicolor quantitative confocal imaging cytometry. *Nat Methods* 2018;**15**:39–46. https://doi.org/10.1038/nmeth.4503
20. Aoyagi Y, Kawakami R, Osanai H, *et al*. A rapid optical clearing protocol using 2,2′-thiodiethanol for microscopic observation of fixed mouse brain. *PLoS One* 2015;**10**:e0116280–13. https://doi.org/10.1371/journal.pone.0116280
21. Omatsu Y, Seike M, Sugiyama T, *et al*. Foxc1 is a critical regulator of haematopoietic stem/progenitor cell niche formation. *Nature* 2014;**508**:536–40. https://doi.org/10.1038/nature13071
22. Seike M, Omatsu Y, Watanabe H, *et al*. Stem cell niche-specific Ebf3 maintains the bone marrow cavity. *Genes Dev* 2018;**32**:359–72. https://doi.org/10.1101/gad.311068.117
23. Pietras EM, Reynaud D, Kang YA, *et al*. Functionally distinct subsets of lineage-biased multipotent progenitors control blood production in normal and regenerative conditions. *Cell Stem Cell* 2015;**17**:35–46.
24. Chen K, Liu J, Chasis JA, *et al*. Resolving the distinct stages in erythroid differentiation based on dynamic changes in membrane protein expression during erythropoiesis. *Proc Natl Acad Sci* 2009;**106**:17413–8.
25. Zhao H, Konishi A, Fujita Y, *et al*. Lipocalin 2 bolsters innate and adaptive immune responses to blood-stage malaria infection by reinforcing host iron metabolism. *Cell Host Microbe* 2012;**12**:705–16. https://doi.org/10.1016/j.chom.2012.10.010
26. Belyaev NN, Brown DE, Diaz AIG, *et al*. Induction of an IL7-R+ c-Kithi myelolymphoid progenitor critically dependent on IFN-γ signaling during acute malaria. *Nat Immunol* 2010;**11**:477–85. https://doi.org/10.1038/ni.1869
27. Wilmore JR, Gaudette BT, Gomez Atria D, *et al*. Commensal microbes induce serum IgA responses that protect against polymicrobial sepsis. *Cell Host Microbe* 2018;**23**:302–311.e3. https://doi.org/10.1016/j.chom.2018.01.005
28. Lemke A, Kraft M, Roth K, *et al*. Long-lived plasma cells are generated in mucosal immune responses and contribute to the bone marrow plasma cell pool in mice. *Mucosal Immunol* 2016;**9**:83–97. https://doi.org/10.1038/mi.2015.38
29. Wilmore JR, Gaudette BT, Gómez Atria D, *et al*. IgA plasma cells are long-lived residents of gut and bone marrow that express isotype- and tissue-specific gene expression patterns. *Front Immunol* 2021;**12**:1–13.
30. Pracht K, Meinzinger J, Daum P, *et al*. A new staining protocol for detection of murine antibody-secreting plasma cell subsets by flow cytometry. *Eur J Immunol* 2017;**47**:1389–92. https://doi.org/10.1002/eji.201747019
31. Koike T, Fujii K, Kometani K, *et al*. Progressive differentiation toward the long-lived plasma cell compartment in the bone marrow. *J Exp Med* 2023;**220**:e20221717. https://doi.org/10.1084/jem.20221717
32. Jian JY, Inoue SI, Bayarsaikhan G, *et al*. CD49d marks Th1 and Tfh-like antigen-specific CD4+ T cells during *Plasmodium chabaudi* infection. *Int Immunol* 2021;**33**:409–22. https://doi.org/10.1093/intimm/dxab020
33. Baldridge MT, King KY, Boles NC, *et al*. Quiescent haematopoietic stem cells are activated by IFN-γ in response to chronic infection. *Nature* 2010;**465**:793–7. https://doi.org/10.1038/nature09135
34. MacNamara KC, Jones M, Martin O, *et al*. Transient activation of hematopoietic stem and progenitor cells by IFNγ during acute bacterial infection. *PLoS One* 2011;**6**:e28669. https://doi.org/10.1371/journal.pone.0028669
35. Florez MA, Matatall KA, Jeong Y, *et al*. Interferon gamma mediates hematopoietic stem cell activation and Niche relocalization through BST2. *Cell Rep* 2020;**33**:108530. https://doi.org/10.1016/j.celrep.2020.108530
36. Crane GM, Jeffery E, Morrison SJ. Adult haematopoietic stem cell niches. *Nat Rev Immunol* 2017;**17**:573–90. https://doi.org/10.1038/nri.2017.53
37. Morikawa S, Mabuchi Y, Kubota Y, *et al*. Prospective identification, isolation, and systemic transplantation of multipotent mesenchymal stem cells in murine bone marrow. *J Exp Med* 2009;**206**:2483–96. https://doi.org/10.1084/jem.20091046
38. Omatsu Y, Aiba S, Maeta T, *et al*. Runx1 and Runx2 inhibit fibrotic conversion of cellular niches for hematopoietic stem cells. *Nat Commun* 2022;**13**:1–12.
39. Nombela-Arrieta C, Isringhausen S. The role of the bone marrow stromal compartment in the hematopoietic response to microbial infections. *Front Immunol* 2017;**7**:1–12.
40. Burberry A, Zeng MY, Ding L, *et al*. Infection mobilizes hematopoietic stem cells through cooperative NOD-like receptor and toll-like receptor signaling. *Cell Host Microbe* 2014;**15**:779–91. https://doi.org/10.1016/j.chom.2014.05.004
41. Isringhausen S, Mun Y, Kovtonyuk L, *et al*. Chronic viral infections persistently alter marrow stroma and impair hematopoietic stem cell fitness. *J Exp Med* 2021;**218**:e20192070. https://doi.org/10.1084/jem.20192070
42. Nakatani T, Sugiyama T, Omatsu Y, *et al*. Ebf3+ niche-derived CXCL12 is required for the localization and maintenance of hematopoietic stem cells. *Nat Commun* 2023;**14**:1–12.
43. Terashima A, Okamoto K, Nakashima T, *et al*. Sepsis-induced osteoblast ablation causes sepsis-induced osteoblast ablation. *Immunity* 2016;**44**:1434–43. https://doi.org/10.1016/j.immuni.2016.05.012
44. Day RB, Bhattacharya D, Nagasawa T, *et al*. Granulocyte colony-stimulating factor reprograms bone marrow stromal cells to actively suppress B lymphopoiesis in mice. *Blood* 2015;**125**:3114–7. https://doi.org/10.1182/blood-2015-02-629444
45. Lightman SM, Utley A, Lee KP. Survival of long-lived plasma cells (LLPC): piecing together the puzzle. *Front Immunol* 2019;**10**:1–12.
46. Lee MSJ, Inoue T, Ise W, *et al*. B cell-intrinsic TBK1 is essential for germinal center formation during infection and vaccination in mice. *J Exp Med* 2022;**219**:e20211336. https://doi.org/10.1084/jem.20211336
47. Maltha J, Guiraud I, Kabore B, *et al*. Frequency of severe malaria and invasive bacterial infections among children admitted to a rural hospital in Burkina Faso. *PLoS One* 2014;**9**:1–8.
48. Marie N, Palacpac Q, Ishii KJ, *et al*. Parasitology International Immune tolerance caused by repeated *P. falciparum* infection against SE36 malaria vaccine candidate antigen and the resulting limited polymorphism. *Parasitol Int* 2024;**99**:102845.
49. Dizon BLP, Pierce SK. The tangled web of autoreactive B cells in malaria immunity and autoimmune disease. *Trends Parasitol* 2022;**38**:379–89. https://doi.org/10.1016/j.pt.2022.01.005

50. Amo L, Kole HK, Scott B, *et al. Plasmodium* curtails autoimmune nephritis via lasting bone marrow alterations, independent of hemozoin accumulation. *Front Immunol* 2023;**14**:1–15.
51. Lee MSJ, Natsume-Kitatani Y, Temizoz B, *et al.* B cell-intrinsic MyD88 signaling controls IFN-γ-mediated early IgG2c class switching in mice in response to a particulate adjuvant. *Eur J Immunol* 2019;**49**:1433–40. https://doi.org/10.1002/eji.201848084
52. Topazian HM, Gumbo A, Puerto-Meredith S, *et al.* Asymptomatic *Plasmodium falciparum* malaria prevalence among adolescents and adults in Malawi, 2015–2016. *Sci Rep* 2020; **10**:1–11.
53. Silva-Filho JL, Lacerda MVG, Recker M, *et al. Plasmodium vivax* in hematopoietic niches: hidden and dangerous. *Trends Parasitol* 2020;**36**:447–58. https://doi.org/10.1016/j.pt.2020.03.002